Synthesis and Fatigue Life Optimization of a Spring-Less Compliant Robot Leg Design

Rohan Vijay Khatavkar and Ajay Pandit Bhattu

1 Introduction

Legged mobile robots are advantageous over wheeled mobile robots in applications such as search and rescue during fires or earthquakes [1]. This is because the mobility of legged robots is more robust to varying tough terrains (encountered during search and rescue) than wheeled robots [2].

Many state-of-the-art legged robots have legs built with springs along with rigid links like in [3, 4] or rigid links with parallel hydraulic actuators like in [5–7]. Though such leg designs mimic the kinematics, elastics, and dynamics of animal locomotion, they generally make the leg assembly complex and expensive.

On the other hand, if compliant mechanisms are used to build legs, their inherent kinematic, elastic, and dynamic behavior may be exploited to mimic animal legs and simplify the leg assembly along with its control strategies. Moreover, compliant mechanism-based leg designs have previously been used in meso-scale-legged robots [8–10]. Further, [11], which uses such a design in a macro-scale-legged robot, provides only a single degree of freedom which limits the implementation of multiple gaits in the robot. Therefore, compliant mechanism based robot legs with multiple degrees of freedom need to be explored more.

In summary, the simplified leg assembly due to a compliant mechanism-based leg design in macro-scale-legged robots may, in turn, reduce the legs' weight, cost, and effort and time for replacement in critical situations. Thus, we report a two degree of freedom compliant mechanism-based robot leg design in the following sections.

R. V. Khatavkar (✉) · A. P. Bhattu
College of Engineering Pune, Pune, India
e-mail: khatavkarrv19.mech@coep.ac.in

A. P. Bhattu
e-mail: apb.mech@coep.ac.in

P. Pradeep Pratapa et al. (eds.), *Advances in Multidisciplinary Analysis and Optimization*,
Lecture Notes in Mechanical Engineering,
https://doi.org/10.1007/978-981-19-3938-9_48

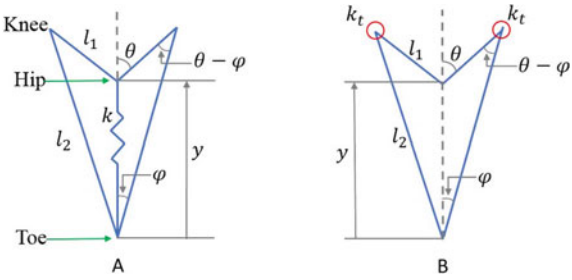

Fig. 1 **a** Leg design by Kenneally and Koditschek; **b** Torsional spring-loaded linkage equivalent to (**a**)

2 Methodology

2.1 Selection of the Linkage to be Converted into Compliant

As there are many spring-loaded rigid robot legs designs reported in robotics literature, it is reasonable to convert one of them into a compliant mechanism. This is because such a design could make the implementation of well-developed legged robot locomotion principles easier. Thus, the following designs reported earlier were considered.

In series elastic actuator-based leg designs like [3], all the actuating motors are placed at the hip, and the knee joint is actuated using chain drives to reduce the leg inertia. Strategies to eliminate the chain drive would have led to reduced actuated degrees of freedom making the control algorithm complicated, and thus, other similar designs were not considered. Parallel linkages on the other hand are actuated only at the hip by two motors. Hence, the coil spring-loaded symmetric five bar rigid robot leg design in [12] shown in Fig. 1a was found to be suitable for conversion into a compliant linkage. The linkage has a zero-length fixed link with two coaxial motors at the hip.

The referred rigid leg geometry, topology, and its stiffness have been optimized in [13] to maximize the transduction of battery energy to body energy during stance, minimize the collision losses upon toe touchdown, and maximize the storage and harvest of prior body energy in spring during stance. The optimization led to $k = 1565\text{N/m}$ on assuming $l_1 = 0.1\text{m}$, $l_2 = 0.2\text{m}$ and mass supported by the leg $M = 1.85\text{kg}$. Thus, the compliant linkage must not deviate from the original geometry or the overall leg stiffness, i.e., the compliant linkage must be kinematically and dynamically equivalent to the rigid linkage.

2.2 Synthesis of the Compliant Linkage

The pseudo-rigid body model of a compliant linkage consists of rigid links with revolute joints and a torsion spring at the rigid joints. Thus, the coil spring-loaded

rigid linkage was converted to a rigid linkage with torsion springs at the two knee joints as in Fig. 1b. To preserve the leg kinematics, the link lengths l_1 and l_2 were maintained the same. The torsional spring stiffness to preserve dynamic equivalence was determined as follows. Refer Fig. 1b.

$$l_2 \sin\varphi = l_1 \sin\theta \tag{1}$$

$$l_2 \cos\varphi - y = l_1 \cos\theta \tag{2}$$

The knee joint angle $\theta - \varphi$ in terms of the vertical coordinate y and link lengths

$$\begin{aligned} \theta - \varphi = \cot^{-1}\left(\frac{-l_1^2 + l_2^2 - y^2}{\sqrt{-l_1^4 - \left(l_2^2 - y^2\right)^2 + 2l_1^2\left(l_2^2 + y^2\right)}}\right) \\ -cot^{-1}\left(\frac{-l_1^2 + l_2^2 + y^2}{\sqrt{-l_1^4 - \left(l_2^2 - y^2\right)^2 + 2l_1^2\left(l_2^2 + y^2\right)}}\right) \end{aligned} \tag{3}$$

Assuming horizontal position of the links of length l_1 corresponds to rest angle of the torsional springs at $y = y_0 = 0.17$m, the knee joint torque

$$T = k(y - y_0) l_1 \sin\theta \tag{4}$$

The knee joint torque in terms of y and link lengths

$$T = \frac{k}{2}\sqrt{-l_1^4 - \left(l_2^2 - y^2\right)^2 + 2l_1^2\left(l_2^2 + y^2\right)} \tag{5}$$

Knee joint torque (parameterized by y) v knee joint angular deflection from rest angle (parameterized by y) was plotted and observed to be fairly linear in Fig. 2. As y_0 corresponds to torsional spring rest angle, the plot was linearized at $y_0 = 0.1732$m (red dot) to determine the required torsional stiffness $k_t = 7.826$Nm/rad.

The torsional spring-loaded rigid linkage was converted into four possible compliant linkages with the pseudo-rigid body method from [14]:

- compliant linkage with a small length flexure (SLF) along the link of length l_1 at the knee (variation A, Fig. 3a) or
- compliant linkage with a small length flexure (SLF) along the link of length l_2 at the knee (variation B, Fig. 3b) or
- compliant linkage with a slender beam (distributed compliance) along the link of length l_1 (variation C, Fig. 3c) or
- compliant linkage with a slender beam (distributed compliance) along the link of length l_2 (variation C, Fig. 3d) or

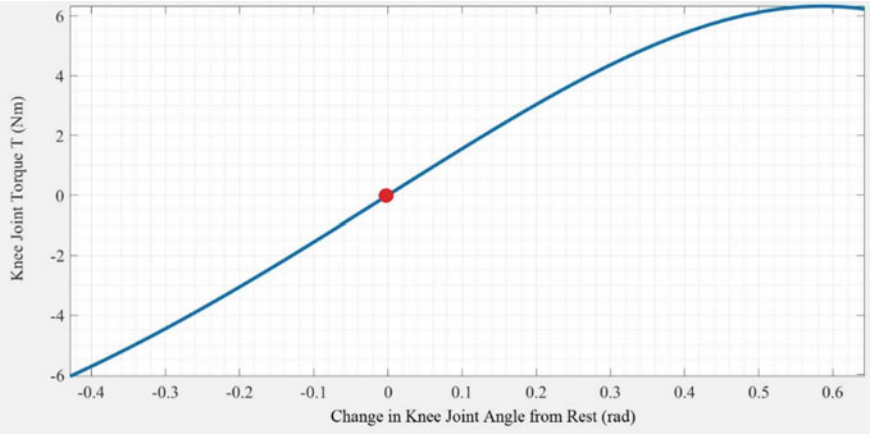

Fig. 2 Desired knee joint torque vs angular deflection

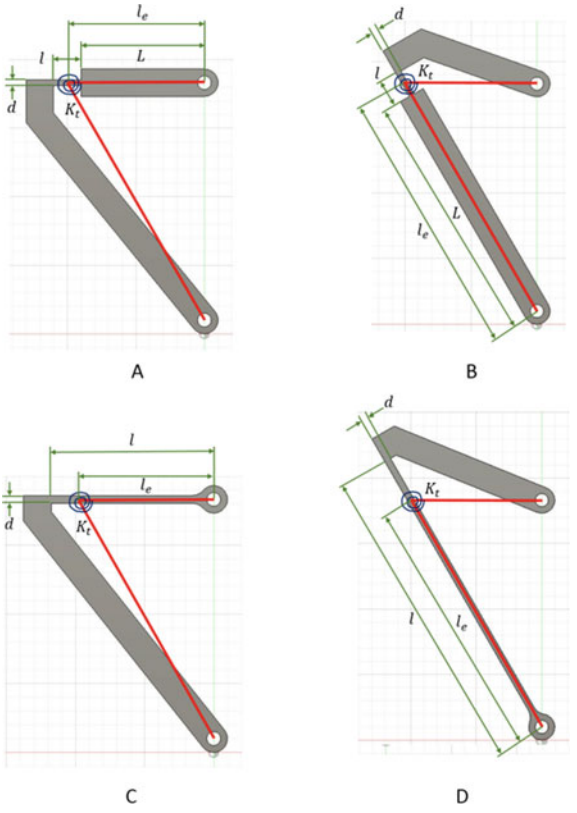

Fig. 3 **a**, **b**, **c,** and **d** Four compliant linkage variations synthesized based on the rigid linkage using pseudo-rigid body method

Table 1 Pseudo-rigid body method-based dimensions of the four variations

Variation	l	I	d
A	$l = 20\text{mm}, L = l_e - \frac{l}{2}$	$I = \frac{K_t l}{E}$	$d = \sqrt[3]{\frac{121}{b}}$
B	$l = 20\text{mm}, L = l_e - \frac{l}{2}$	$I = \frac{K_t l}{E}$	$d = \sqrt[3]{\frac{121}{b}}$
C	$l = \frac{l_e}{0.85}$	$I = \frac{K_t l}{2.25E}$	$d = \sqrt[3]{\frac{121}{b}}$
D	$l = \frac{l_e}{0.85}$	$I = \frac{K_t l}{2.25E}$	$d = \sqrt[3]{\frac{121}{b}}$

ABS ($E = 2.28\text{MPa}$) was assumed as the build material. l_1 and l_2 for all the four compliant linkage variations were the same as the spring-loaded rigid linkages. The depth (into the paper) b in Fig. 3 was assumed to be 10 mm for all the variations. The length of the small length flexures in variations A and B was assumed to be 20 mm. The lengths of the slender regions equivalent to the torsional spring-loaded rigid links were determined using pseudo-rigid body models in [14]. (Refer Table 1 and Fig. 3) The moment of inertia I of the slender regions of the variations was determined for obtaining the required stiffness k_t. Further, the thickness d of the slender regions in Fig. 3 for the variations was determined.

The four variations were numerically evaluated for their kinematic and dynamic equivalence with the rigid linkage using finite element method. The kinematic equivalence was verified by comparing the knee joint trajectory of the rigid linkage with that of the location corresponding to the pseudo-knee joint in the compliant linkage when the hip was vertically loaded, and toe was grounded. (Fig. 4 shows the compliant leg motion). The stiffness between the hip and the toe joint of the compliant linkage was compared with the stiffness of the coil spring for the dynamic equivalence.

3 Results

The numerical evaluation of the kinematic equivalence in Fig. 5a revealed that the four variations were lying within a maximum of -3% deviation from the rigid linkage. The dynamic equivalence evaluation in Fig. 5b revealed that the compliant variation D deviated the least (19.43% maximum) from the rigid linkage. Further, its fatigue life was optimized by maximizing the cross-sectional area a in Eq. (7) of the compliant link constrained by maintaining a constant area moment of inertia I in Eq. (8) and minimum thickness possible in FDM in Eq. (9). Fatigue life was determined using [15]:

$$\text{Stress Amplitude} = 164.28 \times (\text{Cycles to Failure})^{-0.199} \tag{6}$$

Maximize

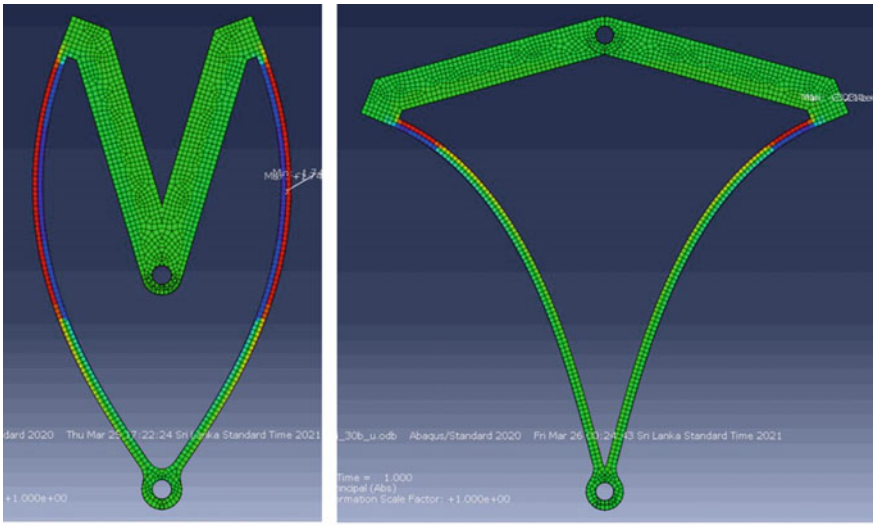

Fig. 4 Dynamic simulation of variation D

$$a = b \times d \tag{7}$$

Subjected to

$$I = \frac{bd^3}{12} = 304.8 \text{ mm}^4 \tag{8}$$

$$d \geq 5 \text{ mm} \tag{9}$$

This optimization resulted in 6x improvement (initial $b = 10$mm) in fatigue life at $b = 30$mm as observed from Table 2. The optimization affected the kinematic equivalence negligibly as observed in Fig. 6a. The optimization of fatigue life also led to an improved dynamic equivalence with the maximum stiffness deviation reducing from 19.43% to 12.69% as observed in Fig. 6b

4 Conclusion

Two revolute joints and the coil spring in the rigid linkage were eliminated to simplify the assembly by using a 3-bar compliant structure. This structure's dynamic and kinematic equivalence to the rigid linkage implies simpler implementation of the control strategies developed for the rigid-legged robot in the compliant-legged robot. The deviations in the kinematics and dynamics of the compliant linkage from the

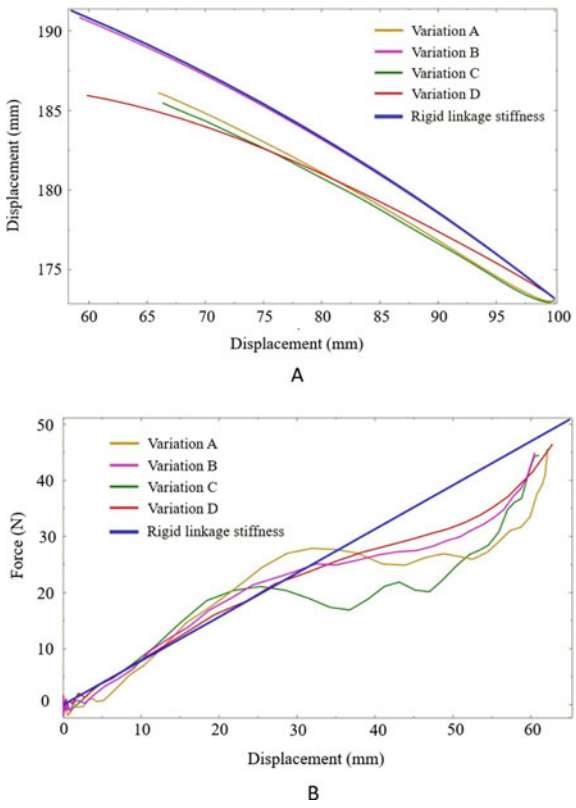

Fig. 5 **a** Comparison of kinematic equivalence of the four compliant linkage variations with the rigid linkage; **b** Comparison of dynamic equivalence

Table 2 Effect of increasing the depth of the compliant variation D

Depth (b) (mm)	Max stress (MPa)	Min stress (MPa)	Stress amplitude (MPa)	Life (cycles)
10	32.92	−34.49	33.705	2862
15	29.91	−21.91	25.91	10,733
20	31.64	−19.59	25.615	11,369
25	32.02	−17.41	24.715	13,607
30	31.11	−15.56	23.335	18,162

spring-loaded rigid linkage were lower when the longer link was made compliant (variations B and D) instead of the shorter link (variations A and C). This is because the longer link undergoes a smaller rotation during the full range of motion of the linkage, and the deviation of pseudo-rigid body models increases with increasing deflection. The stress amplitude was also minimum in this case. This is because it is subjected to a larger axial force than normal force. Further, fatigue life optimization led to a 6x increase in the fatigue life of the compliant linkage.

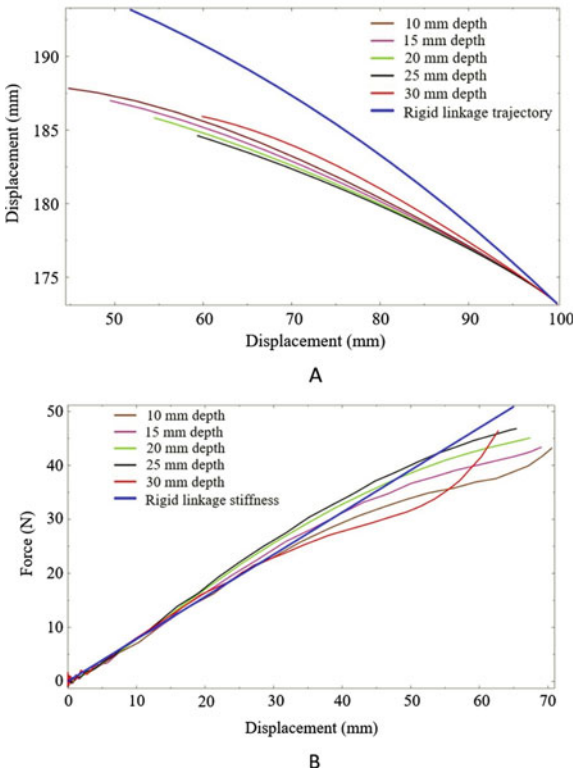

Fig. 6 **a** Effect of increasing depth of the compliant variation D on its kinematic equivalence with rigid linkage; **b** Effect on dynamic equivalence

References

1. Bellicoso CD et al (2018) Advances in real-world applications for legged robots. J Field Robot 35(8):1311–1326. https://doi.org/10.1002/ROB.21839
2. Rubio F, Valero F, Llopis-Albert C (2019) A review of mobile robots: concepts, methods, theoretical framework, and applications. Int J Adv Robot Syst 16(2). https://doi.org/10.1177/1729881419839596
3. Hutter M, Remy CD, Hoepflinger MA, Siegwart R ScarlETH: design and control of a planar running robot. IEEE international conference on intelligent robots and systems, pp 562–567. https://doi.org/10.1109/IROS.2011.6048146
4. Masia L et al ()2018 Oncilla robot: a versatile open-source quadruped research robot with compliant pantograph legs. Frontiers in Robotics and AI, vol 1, p 67. www.frontiersin.org. https://doi.org/10.3389/frobt.2018.00067
5. Semini C, Tsagarakis NG, Vanderborght B, Yang Y, Caldwell DG (2008) HyQ—hydraulically actuated quadruped robot: Hopping leg prototype. In Proceedings of the 2nd Biennial IEEE/RAS-EMBS international conference on biomedical robotics and biomechatronics, BioRob 2008, pp 593–599. https://doi.org/10.1109/BIOROB.2008.4762913
6. Semini C et al (2017) Design of the hydraulically actuated, torque-controlled quadruped robot HyQ2Max. IEEE/ASME Trans Mechatron 22(2):635–646. https://doi.org/10.1109/TMECH.2016.2616284
7. Products|Boston Dynamics. https://www.bostondynamics.com/products. Accessed 24 Jan 2022

8. Jung GP, Choi HC, Cho KJ (2017) The effect of leg compliance in multi-directional jumping of a flea-inspired mechanism. Bioinspir Biomim 12(2):026006. https://doi.org/10.1088/1748-3190/AA575A
9. Zhou X, Bi S (2012) A survey of bio-inspired compliant legged robot designs. Bioinspir Biomim 7(4):041001. https://doi.org/10.1088/1748-3182/7/4/041001
10. Hoffman KL, Wood RJ (2011) Passive undulatory gaits enhance walking in a myriapod millirobot. In 2011 IEEE/RSJ international conference on intelligent robots and systems, pp 1479–1486. https://doi.org/10.1109/IROS.2011.6094700
11. Saranli U, Buehler M, Koditschek DE (2001) RHex: a simple and highly mobile hexapod robot. Int J Robot Res 20(7):616–631. https://doi.org/10.1177/02783640122067570
12. Kenneally G, Koditschek DE Kinematic leg design in an electromechanical robot. kodlab.seas.upenn.edu
13. Kenneally G, Koditschek DE (2015) Leg design for energy management in an electromechanical robot. In: IEEE/RSJ international conference on intelligent robots and systems (IROS), vol 2015-December, pp 5712–5718. https://doi.org/10.1109/IROS.2015.7354188
14. Howell LL, Magleby SP, Olsen BM (2013) Handbook of compliant mechanisms. Handb Compliant Mech. https://doi.org/10.1002/9781118516485
15. Domingo-Espin M, Travieso-Rodriguez JA, Jerez-Mesa R, Lluma-Fuentes J (2018) Fatigue performance of ABS specimens obtained by fused filament fabrication. Materials 11(12):2521. https://doi.org/10.3390/MA11122521